

***Ab initio* calculations of the electronic structure and bonding characteristics of LaB₆**Faruque M. Hossain,* Daniel P. Riley,[†] and Graeme E. Murch*School of Engineering, The University of Newcastle, Callaghan, New South Wales 2308, Australia*

(Received 22 March 2005; revised manuscript received 29 July 2005; published 1 December 2005)

Lanthanum hexaboride (LaB₆, NIST SRM-660a) is widely used as a standard reference material for calibrating the line position and line shape parameters of powder diffraction instruments. The accuracy of this calibration technique is highly dependent on how completely the reference material is characterized. Critical to x-ray diffraction, this understanding must include the valence of the La atomic position, which in turn will influence the x-ray form factor (f) and hence the diffracted intensities. The electronic structure and bonding properties of LaB₆ have been investigated using *ab initio* plane-wave pseudopotential total energy calculations. The electronic properties and atomic bonding characteristics were analyzed by estimating the energy band structure and the density of states around the Fermi energy level. The calculated energy band structure is consistent with previously reported experimental findings; de Haas-van Alphen and two-dimensional angular correlation of electron-positron annihilation radiation. In addition, the bond strengths and types of atomic bonds in the LaB₆ compound were estimated by analyzing the Mulliken charge density population. The calculated result revealed the coexistence of covalent, ionic, and metallic bonding in the LaB₆ system and partially explains its high efficiency as a thermionic emitter.

DOI: [10.1103/PhysRevB.72.235101](https://doi.org/10.1103/PhysRevB.72.235101)

PACS number(s): 71.15.Ap, 31.15.Ar, 31.15.Ew, 61.10.Nz

I. INTRODUCTION

X-ray powder diffraction is widely applied in the fields of biology, materials science, and physics. It is a versatile technique for accurately determining such quantities as crystal structures, lattice parameters, bond geometries, residual strain, or average crystallite size. These quantities are best determined using Rietveld analysis, a computational technique that relies on a detailed model of the atomic structure.¹ Neglecting source stability and wavelength variances, the accuracy of this method relies primarily on determining the contributions of the instrument independent of the sample being analyzed. Although the instrumental contributions may be calculated, the high number and variability of factors affecting such estimates mean it is more practical to measure these influences using a standardized powder sample. Furthermore, as instrumental geometries are often matched to the characteristics of the experiment, the use of a standard reference material allows for direct comparison between different instruments or experimental apparatus.

In general, the accuracy of this “*instrumental calibration*” using a standard reference material is dependent on how well the material is characterized. To this end, several powder diffraction reference materials have been developed by the National Institute of Standards and Technology (NIST), including lanthanum hexaboride, LaB₆ (NIST Standard Reference Material SRM-660a).² Recent attempts at characterizing this material have aimed at improving its suitability as a standard reference material for x-ray powder diffraction (XRD). This includes, amongst other work, precise measurement of the LaB₆ lattice spacing using synchrotron radiation³ and investigation of the residual crystallite strain inherent in SRM-660a material.⁴

Despite this interest, disagreement remains over the electronic structure of this compound, in particular, the effective valence state of La, which may be either neutral or La⁺. This is critical since the x-ray form factor (f) is altered by the

valence of that element. Furthermore, conjecture over this valence state prevents either a better understanding of *pseudometallic* characteristics attributed to LaB₆ (Refs. 5 and 6), or an explanation of conflicting conclusions drawn by Tanaka *et al.*⁷ concerning the *ionic* nature of the charge transfer between La and B atoms. In the former, Walch *et al.* used a discrete variational method of the *Hartree-Fock-Slater* model to calculate the energy bands of LaB₆, concluding that the La-B atomic bonding was covalent and more significant to overall bonding than La-La interactions.⁵ On the other hand, Tanaka *et al.*, using electrical resistivity measurements, observed a considerable charge transfer between La and B, attributing the “*metallic*” conduction to polar optical phonon scattering within the ionic structure, namely LaB₆.⁷ In retrospect, the actual bonding of LaB₆ could at best be described as uncertain. In order to further develop LaB₆ as a standard reference material for x-ray powder diffraction it is therefore important to understand the mechanisms of bonding that exist in this material. In this paper we have investigated the electronic structure of LaB₆ in an attempt to answer these questions.

II. CRYSTAL STRUCTURE AND METHOD OF CALCULATION

The crystal structure of LaB₆ is simple cubic (space group; *Pm-3m*), with B₆-octahedra in body-centered positions and La atoms at the corners of the unit cell. An illustrative crystal structure of LaB₆, comprised of two unit cells, is shown in Fig. 1. Boron atoms in the two octahedral cages have been numerically labeled (B1, B2, ..., B11, B12) in order to assist the discussion of the bonding characteristics of LaB₆. The $2a \times 2b \times 2c$ supercell of LaB₆ was used for the electronic structure calculation and Mulliken charge density population calculation. The lattice parameters were geometrically optimized and the ground-state electronic struc-

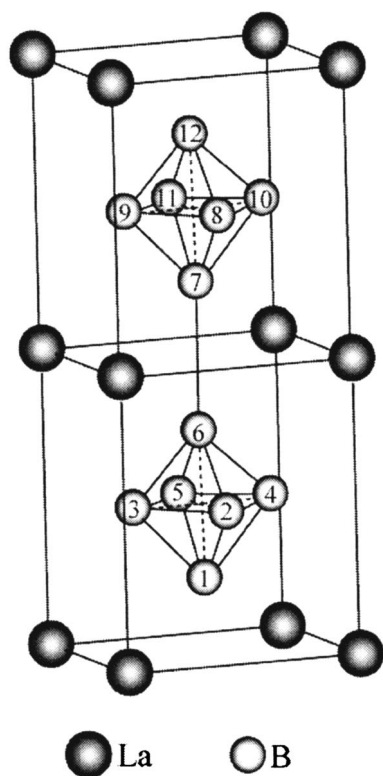


FIG. 1. The crystal structure of Lanthanum hexaboride. Two unit cells are shown in order to represent the bonding between two adjacent octahedral (B_6-B_6). The bond length of B_6-B_7 is the shortest distance in the structure.

ture calculated using the CASTEP software code.^{8,9} The CASTEP code utilizes a plane-wave (PW) pseudopotential total energy calculation method based on density functional theory (DFT), as described thoroughly in the literature.¹⁰⁻¹² The electronic wave functions were expanded in a PW with a 330 eV basis cutoff, which was deemed sufficient for convergence of the total energy calculation. The valence states for La and B were $5s^2$, $5p^6$, $5d^1$, $6s^2$, and $2s^2$, $2p^1$, respectively. The electronic exchange-correlation energy was imposed into the total energy calculation through the generalized gradient approximation (GGA) scheme.¹³ A Monkhorst-Pack mesh¹⁴ of $6 \times 6 \times 6$ special k points was chosen for sampling, while calculations for the partial density of states (PDOS) were performed using a projection of the PW states onto a localized linear combination of atomic orbitals (LCAO) basis set. Mulliken charges and bond overlap populations were calculated by projecting the PW Kohn-Sham eigenstates onto the atomic basis sets. Projection of the PW states onto a LCAO basis set¹⁵ was used to perform Mulliken population calculations. Population analysis of the resulting projected states is then performed using the Mulliken formalism.¹⁶ According to the Mulliken formalism the quality of the PW states projection is evaluated by calculating a charge spilling parameter, which provides a measure of reliability for this calculation. The charge spilling parameter in our calculation is 1.9×10^{-3} , which indicates that an acceptable 0.19% of the valence has been lost in the projection.

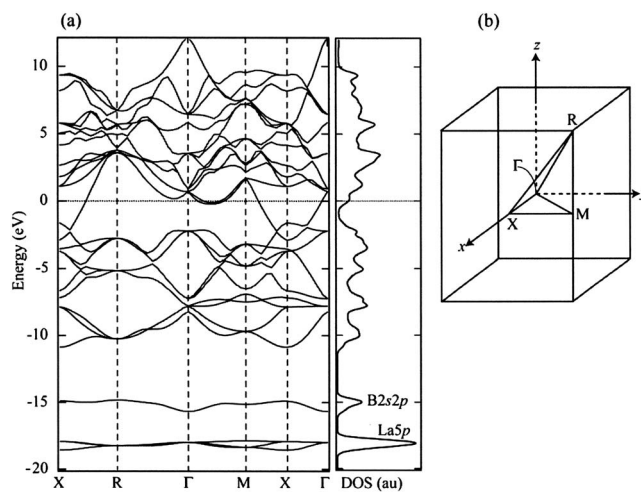


FIG. 2. (a) Band structure and total DOS of LaB_6 supercell. Dotted line at zero energy level indicates the Fermi level. (b) Brillouin zone for the simple-cubic Bravais lattice.

III. RESULTS AND DISCUSSION

A. Energy band structure

The energy band structure for LaB_6 was calculated along the high-symmetry directions of the cubic Brillouin zone (BZ), as shown in Fig. 2(a). Figure 2(b) shows the simple-cubic BZ with four (Γ , X , M , and R) high symmetry points. As seen in the Fig. 2(a), the lowest three bands were generated from the La $5p$ state. These bands provide a sharp peak in the density of states compared to the valence and conduction band states. A flat band at -15.0 eV is an isolated part of the valence band arises mainly from an equal contribution of both B $2s$ and $2p$ states, and a small contribution of the La $6s$ states.

The main part of the valence band consists mainly of the B sp states and slightly of the La d state which is completely occupied. The width of the valence band is about 9.0 eV, and it is divided into two parts with the highest density of states (DOS) arising at around 10.0 and 5.0 eV below E_F . These results are in fair agreement with the experimental results for the ultraviolet photoelectron spectroscopy (UPS) spectra of Mori *et al.*¹⁷ and for the x-ray photoemission (XPS) spectra of Chazalviel *et al.*¹⁸

The lowest energy level (14th band, Σ_1) of the conduction band crosses the Fermi level, E_F , along the ΓM direction, while exceeding E_F along the ΓR direction with twofold degeneracy along other high symmetry points in the Brillouin zone. One of the degenerated states crosses E_F and touches with the highest energy states of the valence band along the ΓX , XR , and XM directions with a large dispersion. This particularly large dispersion in the vicinity of the Fermi energy is due to the effect of B sp La d hybridization and is indicative of the light effective mass of the conduction electrons. The main Fermi surfaces corresponding to this 14th band consist of nearly spherical electron ellipsoids centered at X points in the simple cubic Brillouin zone. These ellipsoids are connected with each other via short, thick necks intersecting the Σ axes. Our calculated energy band structure

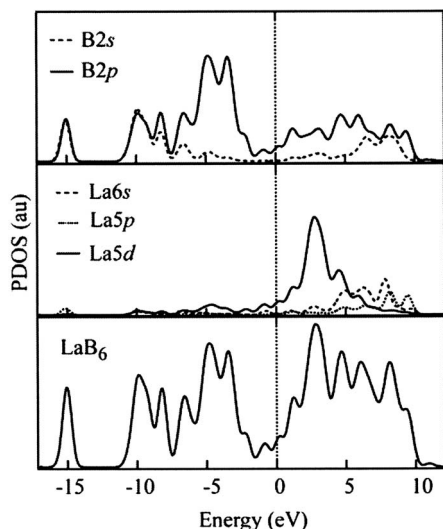


FIG. 3. PDOS of the LaB_6 supercell. Zero line (dotted) represents the Fermi level.

is in good agreement with results of the self-consistent augmented-plane-wave (APW) method of Hasegawa *et al.*,¹⁹ Harima *et al.*,²⁰ and with the full-potential linearized augmented-plane-wave (FLAPW) method of Kubo and Asano.²¹ Interestingly, our method of calculation provides an extra band (15th band, Σ_4) along the ΓM direction that also crosses E_F , indicating the presence of small electron pockets as illustrated clearly in a perspective view of Harima *et al.* [see Fig. 2 in Ref. 20]. In all previous theoretical works of LaB_6 , the topological properties of the Fermi surface were obtained by their calculated band structure, generally agreeing with the dHvA experiments of Arko *et al.*,²² Ishizawa *et al.*,²³ and with recent experimental results on the 2D ACAR of Kontrym-Sznajd *et al.*²⁴ However, these previous calculations failed to directly predict our present observations of small electron pockets in the 15th band along the ΓM direction, which more correctly models the dHvA and 2D ACAR experiments. Harima *et al.* obtained these elements by tentatively shifting the $4f$ level upward by 0.1 Ry. In our calculation we successfully produced these elements without including either the $4f$ orbital or considering energy shifts. Consequently, our energy band structure more thoroughly describes the observation of the de Haas-van Alphen (dHvA) and two-dimensional angular correlation of electron-position annihilation radiation (2D ACAR) experiments. Furthermore, as our theoretical results are in strong agreement with previous experiments and illustrate a mixture of valence and conduction band states, they suggest the existence of metallic bonding in LaB_6 . However, it is not absolutely correct to describe the possible bonding structures solely from such observations. In order to obtain further information about the nature of these bonds the PDOS were calculated.

B. Density of states

The calculated PDOS for LaB_6 is shown in Fig. 3. It is clear from the figure that the valence band can be separated into two equal intervals (-1.5 to -7.5 eV and -7.5 to

TABLE I. Atomic Mulliken charges and effective valence charges in LaB_6 calculated from PW electronic structure calculations.

Species	<i>s</i>	<i>p</i>	<i>d</i>	Total (<i>e</i>)	Charge (<i>e</i>)	Effective valence (<i>e</i>)
B	0.86	2.57	0.00	3.43	-0.43	
La	1.51	5.41	1.53	8.45	2.55	+0.45

-11.0 eV). The lower interval originates from almost equal contributions of B $2s$ and $2p$ orbitals, while the upper interval is dominated by the B $2p$ orbital weakly hybridized with La $5d$ orbitals. The B $2p$ state extends into and above the vicinity of the Fermi energy level and shows a strong hybridization with the La $5d$ states. Similarly, the conduction band has two parts (0 to 5.0 eV and 5.0 to 10.0 eV) depending on the weight of the PDOS. The lower part is dominated by La $5d$ hybridized with the B $2sp$ states, while the upper part is populated with unoccupied antibonding (σ^* and π^* bonds) states of both B and La atoms. This result is unable to explain the ionic bonding observed by Tanaka,⁷ but does provide evidence for a covalent structure. Hence, we may suspect the coexistence of both covalent and ionic bonding in this compound. A more detailed understanding of the actual bonding characteristic of this system can be derived from analysis of the Mulliken charge density population.

C. Mulliken population analyses

The Mulliken charge and overlap population are useful in evaluating the covalent, ionic, or metallic nature of bonds in a compound. A high value of the bond population indicates a covalent bond, whilst a low value indicates an ionic nature. Alternatively, the degree of covalency and/or ionicity may be obtained from the effective valence, which is defined as the difference between the formal ionic charge and the Mulliken charge on the cation species.²⁵ A value of zero indicates a perfectly ionic bond, while values greater than zero indicate increasing levels of covalency. Although the physical meaning and scientific interpretation of the values of Mulliken charges or bond populations in metallic systems is not clear, the sign of bonding between atoms is unequivocal.

Table I lists the orbital charges and the effective valence of both the La and B species. The effective valence for La in LaB_6 is +0.45. This value is representative of the concurrent ionic and covalent bonding in LaB_6 . Although it is difficult to put a figure on the level of ionicity and covalency using the effective valence concept, the type of bonding and its level can be determined by calculating the Mulliken bond population.

We may classify two main groups of boron-boron bonds, i.e., $\text{B}_6\text{-B}_6$ and B-B, within the two unit cells of the LaB_6 crystal shown in Fig. 1. The $\text{B}_6\text{-B}_6$ group represents the bonding between two adjacent octahedral atoms, whilst the B-B group represents the bonding between atoms within the same octahedra. The $\text{B}_6\text{-B}_6$ group and B-B groups are further categorized into four [$\text{B}_6\text{-B}_6$ (I); $\text{B}_6\text{-B}_6$ (II); $\text{B}_6\text{-B}_6$ (III); $\text{B}_6\text{-B}_6$ (IV)] and two [B-B (I); B-B (II)] subgroups, respec-

TABLE II. Mulliken bond populations and bond lengths in LaB₆ calculated from PW pseudopotential calculations.

Bond	Bond population, P	Population ionicity, P_i	Bond length (Å)
B ₆ -B ₆ (I) (B6-B7 bond)	1.10	0.00	1.662
B ₆ -B ₆ (II)	-0.07		3.164
B ₆ -B ₆ (III)	0.12	1.00	4.154
B ₆ -B ₆ (IV)	-0.03		4.154
B-B (I)	0.58	0.59	1.762
B-B (II)	-0.52		2.492
La-B (boron nearest to La)	-0.14		3.053
La-La	-1.18		4.154

tively, depending on the bond length. Subgroup B₆-B₆ (I) has one (B6-B7) bond with the shortest bond length in the structure. Subgroup B₆-B₆ (II), B₆-B₆ (III), and B₆-B₆ (IV) have eight (B6-B8; B6-B9; B6-B10; B6-B11; B7-B2; B7-B3; B7-B4; B7-B5), two (B1-B7; B6-B12), and four (B2-B8; B3-B9; B4-B10; B5-B11) bonds, respectively. Similarly, subgroup B-B (I) has 24 (12+12) bonds along the edges of two octahedra and subgroup B-B (II) has six (B1-B6; B3-B4; B2-B5; B7-B12; B9-B10; B8-B11) bonds.

Table II lists the bond populations, population ionicity, and bond lengths for boron-boron, lanthanum-boron, and lanthanum-lanthanum bonds in the LaB₆ crystal. Positive and negative values indicate bonding and antibonding states, respectively. A high positive bond population indicates a high degree of covalency in the bond.²⁵ According to the definition of the ionicity scale of He,²⁶ the population ionicity can be calculated as

$$P_i = 1 - \exp[-|P_c - P|/P],$$

where P is the overlap population of a bond and P_c is the bond population for a purely covalent bond. P_i is equal to zero for a purely covalent bond and to unity for a purely ionic bond. As a reference, the B6-B7 bond (the shortest bond length in the structure) was assumed to be a pure covalent bond with P_c equal to 1.1. The B₆-B₆ (III) bond exhibits almost complete ionicity with slight covalency. Furthermore, the bond B-B (I) shows mixed covalent and ionic characteristics with equal contribution. Hence, it has been observed that covalency and ionicity coexists in the boron “cages” of the LaB₆ octahedra. This result conflicts with the basic concept of ionicity, which states that the ionic nature can only exist when charge transfer occurs between two different atoms. However, it supports the investigation of He²⁶ on the ionicities of boron-boron bonds in B₁₂ icosahedra.

The values of bond population for all other bonds in Table II are negative, indicative of their antibonding nature. It is interesting to note that although the B-B (II) bond in the boron cage shows a repulsive antibonding nature with a bond population of -0.52, the overall resultant bonding remains attractive and keeps the boron structure stabilized. In addition, it is clear from Fig. 3 that B-B (II) antibonding states

located above the Fermi energy level are dominated by B 2*p* (π^* bonds) states.

The coexistence of covalent and ionic bonding in the presence of these antibonding orbitals is further complicated by suggestions of diatomic interactions of electrons, as proposed by Harcourt.²⁷ Specifically, Harcourt advocates that within structures of type $M-M$, where M^+ and M^- bonding coexists in close proximity, an electron from M^- may be delocalized into the vacant, covalent antibonding structure, thereby elevating it into a conductivelike state. Referred to as “metallic orbitals,” similar M sites may be identified in LaB₆, namely $M^- \rightarrow B-B$ (I) (ionic) and $M^+ \rightarrow B-B$ (II) (vacant, covalent antibonding). The adjacency of these M sites within LaB₆ suggests it is possible for electron delocalization to occur under the influence of an electric field. Therefore, not only the La metal atom but also the boron cage would contribute to the metallic conduction process of LaB₆.

Overall, lanthanum has no appreciable bonding interaction with the nearest boron of the B₆ cage (bond population of -0.14), which conflicts with the observation of Tanaka *et al.*⁷ concerning the ionic nature of the charge transfer between La and B atoms. This suggests that La ions are independently immersed within a rigid boron framework. The present calculation of the La-B bonding structure therefore supports a simpler model based on the measurements of LaB₆ specific heat and resistivity established by Mandrus *et al.*²⁸ In basic terms, Mandrus *et al.* proposed that the La ions were independent Einstein oscillators embedded within a rigid boron framework, further simplified as a Debye solid. However, La-La bonds show a high antibonding population of -1.18, similar to the B-B (II) bond. It can be further observed from Fig. 3 that these antibonding states contribute to form an unoccupied conduction band dominated by La 5*d* states. These empty antibonding states could therefore account for the metallic conduction in LaB₆ as 5*d* electrons are transferred into the unoccupied antibonded states in the conduction band when under the influence of an external potential. Furthermore, the valence electrons of the metal atoms are repelled by the “surface potential” of the B₆ octahedra, thus preventing annihilation and enabling conduction of significant free electron densities. It is therefore possible that the majority of the free electron population of LaB₆ is due to antibonding of La 5*d* states and remains conductive due only to the confining potential of similarly stabilized B octahedra.

Overall, the antibonding repulsions of La-B and La-La bonds may help explain the earlier work of Lafferty,²⁹ who noted the high efficiency of LaB₆ as a thermionic emitter. According to Lafferty, such high efficiency resulted from the ability of La atoms to freely migrate through the boride matrix in order to replace those La atoms evaporated from the surface. In explanation, it is possible that the repulsive nature of the La-B and La-La bonds provides an effective “isolation” between the boron sublattice and individual La atoms, thereby enabling ready migration of La atoms through the boride matrix once a vacant site has been established through surface evaporation. If it were not for this effective repulsion of La-B bonding, La mobility would not be as high and would therefore prevent the rapid repopulation of vacant La surface sites.

IV. CONCLUSIONS

Calculation of electronic band structure, DOS, and Mulliken charge population from the PW pseudopotential total energy calculations have provided useful information about the Fermi-surface topology including the presence of small electron pockets, as recently observed by experiment, and on the bonding properties of LaB₆ material.

Previous theoretical works were unable to detect such small electron pockets (15th band) unless they included and shifted the unoccupied 4*f* energy levels. This shift may correspond to the local-density approximation (LDA) considered in the previous calculation. In our band structure calculation (representative of the Fermi-surface topology), we achieved these elements without considering the 4*f* levels and its energy shifts in the band structure. Hence, we may

conclude that the use of the GGA (Ref. 13) functional provides us with a better overall description of the electronic subsystem structure of LaB₆ than the LDA functional. In particular, the calculation suggests that covalent, ionic, and metallic bonds coexist in the LaB₆ crystal structure. We have also provided further supportive evidence of Lafferty's work on the high mobility of lanthanum atoms through the boride matrix.

ACKNOWLEDGMENTS

The authors would like to thank Associate Professor Erich Kisi for numerous discussions on the significance of LaB₆ and acknowledge funding support from the Australian Research Council (Grants Nos. DP451429 and DP0208602).

*Also at the Center for Materials Research in Energy Conversion, School of Materials Science and Engineering, The University of New South Wales, NSW, 2052, Australia.

†Corresponding author Fax: +61 2 49216946. Email address: Daniel.Riley@newcastle.edu.au

¹H. M. Rietveld, *J. Appl. Crystallogr.* **2**, 65, (1969).

²National Institute of Standards and Technology Certificate, Standard Reference Material® 660a, lanthanum hexaboride powder, line position and line shape standard for powder diffraction <http://www.nist.gov/>

³C. T. Chantler, C. Q. Tran, and D. J. Cookson, *Phys. Rev. A* **69**, 042101 (2004).

⁴M. Pitt, (unpublished).

⁵P. F. Walch, D. E. Ellis, and F. M. Mueller, *Phys. Rev. B* **15**, 1859–1866 (1977).

⁶F. A. Cotton and G. Wilkinson, *Advanced Inorganic Chemistry, A Comprehensive Text* edited by Interscience Publishers (Interscience, New York, 1972).

⁷T. Tanaka, T. Akahane, E. Bannai, S. Kawai, N. Tsuda, and Y. Ishizawa, *J. Phys. C* **9**, 1235 (1976).

⁸M. C. Payne, M. P. Teter, D. C. Allan, T. A. Arias, and J. D. Joannopoulos, *Rev. Mod. Phys.* **64**, 1045 (1992).

⁹L. J. Clarke, I. Stich, and M. C. Payne, *Comput. Phys. Commun.* **72**, 14 (1992).

¹⁰P. Hohenberg and W. Kohn, *Phys. Rev.* **136**, B864 (1964).

¹¹W. Kohn and L. J. Sham, *Phys. Rev.* **140**, A1133 (1965).

¹²M. Levy in *Proc. Natl. Acad. Sci. U.S.A.* **76**, 6062 (1979).

¹³J. P. Perdew, K. Burke, and M. Ernzerhof, *Phys. Rev. Lett.* **77**, 3865 (1996).

¹⁴H. Monkhorst and J. D. Pack, *Phys. Rev. B* **13**, 5188 (1976).

¹⁵D. Sanchez-Portal, E. Artacho, and J. M. Soler, *Solid State Commun.* **95**, 685 (1995); *J. Phys.: Condens. Matter* **8**, 3859 (1996).

¹⁶R. S. Mulliken, *J. Chem. Phys.* **23**, 1833 (1955).

¹⁷Y. Mori, N. Shino, S. Imada, S. Suga, T. Nanba, M. Tomikawa, and S. Kunii, *Physica B*, **86-188**, 66 (1993).

¹⁸J.-N. Chazalviel, M. Campagna, G. K. Wertheim, and P. H. Schmidh, *Solid State Commun.* **19**, 725 (1976).

¹⁹A. Hasegawa and A. Yanase, *J. Phys. F: Met. Phys.* **7**, 1245 (1977).

²⁰H. Harima, O. Sakai, T. Kasuya, and A. Yanase, *Solid State Commun.* **66**, 603 (1988).

²¹Y. Kubo and S. Asano, *Phys. Rev. B* **39**, 8822 (1989).

²²A. J. Arko, G. Crabtree, D. Karim, F. M. Mueller, L. R. Windmiller, J. B. Ketterson, and Z. Fisk, *Phys. Rev. B* **13**, 5240 (1976).

²³Y. Ishizawa, T. Tanaka, E. Bannai, and S. Kawai, *J. Phys. Soc. Jpn.* **42**, 112 (1977).

²⁴G. Kontrym-Sznajd, M. Samsel-Czekala, M. Biasini, and Y. Kubo, *Phys. Rev. B* **70**, 125103 (2004).

²⁵M. D. Segall, R. Shah, C. J. Pickard, and M. C. Payne, *Phys. Rev. B* **54**, 16317 (1996).

²⁶J. He, E. Wu, H. Wang, R. Liu, and Y. Tian, *Phys. Rev. Lett.* **94**, 015504 (2005).

²⁷R. D. Harcourt, *J. Phys. B* **7**, L41–L45 (1974).

²⁸D. Mandrus, B. C. Sales, and R. Jin, *Phys. Rev. B* **64**, 012302 (2001).

²⁹J. M. Lafferty *J. Appl. Phys.* **22**, 299 (1951).